NANO LETTERS

pubs.acs.org/NanoLett

Letter

# Dynamic Focusing with High-Quality-Factor Metalenses

Elissa Klopfer,* Mark Lawrence, David R. Barton, III, Jefferson Dixon, and Jennifer A. Dionne*

Cite This: *Nano Lett.* 2020, 20, 5127−5132

Read Online

ACCESS | Metrics & More | Article Recommendations | Supporting Information

**ABSTRACT:** Metasurface lenses provide an ultrathin platform in which to focus light, but weak light−matter interactions limit their dynamic tunability. Here we design submicron-thick, ultrahigh quality factor (high-*Q*) metalenses that enable dynamic modulation of the focal length and intensity. Using full-field simulations, we show that quality factors exceeding 5000 can be generated by including subtle, periodic perturbations within the constituent Si nanoantennas. Such high-*Q* resonances enable lens modulation based on the nonlinear Kerr effect, with focal lengths varying from 4 to 6.5 $\mu$m and focal intensities decreasing by half as input intensity increases from 0.1 to 1 mW/$\mu$m$^2$. We also show how multiple high-*Q* resonances can be embedded in the lens response through judicious placement of the perturbations. Our high-*Q* lens design, with quality factors 2 orders of magnitude higher than existing lens designs, provides a foundation for reconfigurable, multiplexed, and hyperspectral metasurface imaging platforms.

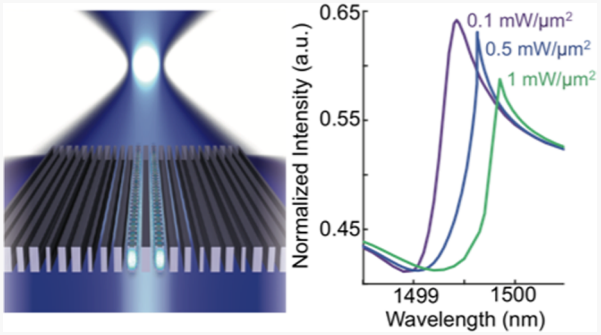


**KEYWORDS:** *Metasurface, metalens, metasurface modulation, high-Q, nonlinearities, nanophotonics*



Metasurface lenses (hereafter, "metalenses") are emerging as key components for next-generation miniaturized and lightweight imaging, sensing, and computation systems. Constructed from arrays of subwavelength nanoantennas with generally submicron thickness, metasurfaces are designed to discretely and precisely modify the amplitude, polarization, and phase of an arbitrary wavefront.[1−4] Metalenses promise applications including compact, high grade imaging for cameras and displays,[5−8] on chip biomedical diagnostics,[9−12] and next generation augmented and virtual reality (AR/VR) devices.[13,14] And beyond simple "flat optical" imaging, metasurface lenses offer opportunities for multicolor focusing and aberration correction,[15−18] as well as polarization-resolved capabilities.[19] Still, to date, most metalens designs are static, with their function being fixed once fabricated.

Recent studies have shown that metasurface properties can be dynamically tuned via modulation techniques including phase change materials,[20−22] electro-optically active materials,[23−27] liquid crystals,[28−31] or mechanical movement of the nanoantenna.[32−36] Many of these schemes rely on altering the complex refractive index ($n$) of either the nanoantenna or the surrounding environment. Since the index change is proportional to the strength of the local electromagnetic field, metasurface modulation depths are generally small, owing to the low quality factor of the constituent nanoantennas.[21,25,29] Moreover, many existing schemes require bulky external components to actuate the metasurface, adding considerable size and weight to the metasurface footprint. To amplify modulation depths while maintaining a small device footprint, it is crucial to amplify refractive index changes though increased metasurface quality factors.

Here, we design high quality factor (high-*Q*) metalenses capable of dynamic focusing. These metalenses leverage highly enhanced electromagnetic fields to increase the modulation depth with even weak $\Delta n$ effects, without increasing the system footprint. Our design is based on patterned silicon (Si), which has a relatively high refractive index of 3.4, is nearly lossless in the infrared, and affords a relatively large third-order nonlinearity based on the optical Kerr effect, with a $\chi^{(3)}$ of $2.8 \times 10^{-18}$ m$^2$/V$^2$.[37,38] We use full-field simulations to design and characterize a high-*Q* metasurface lens based on guided mode resonances (GMR). We show that this design easily enables *Q*'s in the thousands and near-field intensity enhancements exceeding 10,000. Utilizing the nonlinear Kerr effect, we theoretically demonstrate modulation of both the focal intensity and focal length with varying incident intensity. Finally, we show how this platform can be extended to a frequency-multiplexed metasurface, with resonant lensing behavior at three distinct wavelengths spanning the telecom range.

We construct our cylindrical metalens using nanoantennas, in the form of nanobars, that obey a hyperboloidal phase

**Received:** March 30, 2020
**Revised:** June 4, 2020
**Published:** June 4, 2020

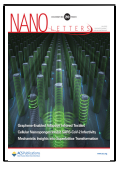

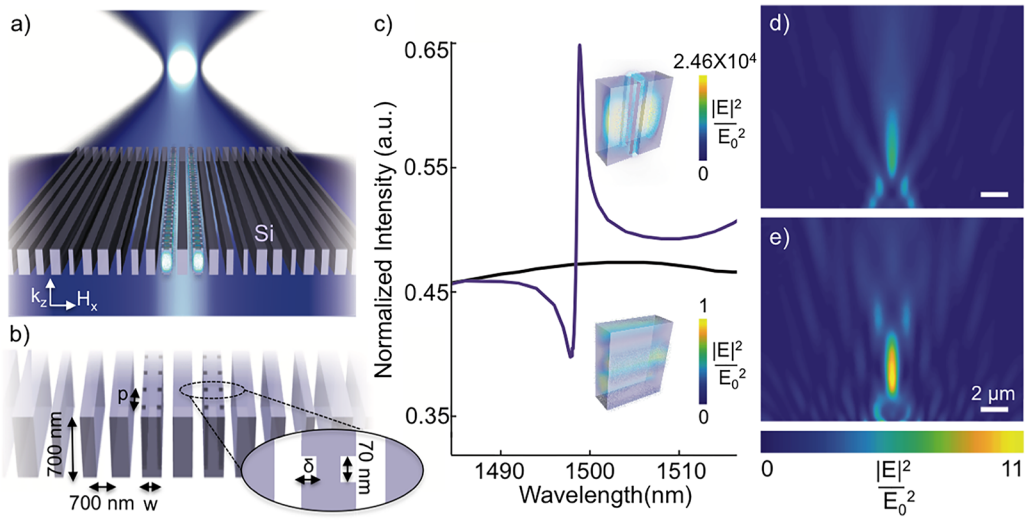


**Figure 1.** High-Q metalens geometry and spectral characteristics. (a) Schematic of the high-Q lens, illustrating the local field enhancements that arise in the notched bars (here positioned on each side of the lens midpoint). (b) Geometry of a subset of the high-Q structure, where $p$ = 600 nm, $\delta$ = 50 nm, and $w$ varies for each bar according to Figure S1b. (c) Spectra of the unnotched (black curve) and notched (purple curve) lenses calculated for the $xy$ plane at the focal spot, 4 $\mu$m from the metasurface. The insets show near-field calculations of the $w$ = 219 nm nanobars for the notched and unnotched lenses. (d) $|E(r)|^2$ field plot for the unnotched lens excited at $\lambda$ = 1499.4 nm and normalized to the mean of the input Gaussian field. (e) $|E(r)|^2$ field plot for the notched, high-Q lens excited at $\lambda$ = 1499.4 nm and normalized to the mean of the input Gaussian field.

profile described by $\phi(x) = \pm\frac{2\pi}{\lambda}(\sqrt{x^2 + f^2} - f)$.[2,4,15] Here, $\lambda$ is the free space wavelength, $x$ is the position of a nanobar, and $f$ is the designed focal length. Individual metasurface nanobars act as phase "pixels", each of which imparts a phase shift dependent on their geometry. We utilize Si nanobars that are 700 nm in height, separated (center-to-center) by 700 nm, with variable widths $w$. By varying the nanobar width from 100 to 400 nm, we achieve a nearly full $2\pi$ phase shift, as shown in Figure S1a. We design the lens to have a 4 $\mu$m focal length at a wavelength of 1500 nm, using 25 discrete nanobars (see Figure S1b for further details of the metasurface dimensions).

To integrate a high-Q resonance into the diffractive metalens, we introduce subtle periodic perturbations along the length of one pair of nanobars, as illustrated in Figure 1a and b. The unperturbed nanobars exhibit broad spectral features associated with Fabry−Perot fringes when illuminated with an incident field traveling perpendicular to the bar. In addition, the nanobars also support wave-guided modes; from the perspective of the external plane wave, the continuous waveguide represents a resonator with infinite $Q$, i.e., a bound state. The inclusion of periodic notches to a nanobar, with the notch period associated with the guided mode wavevector, enables momentum matching and coupling between the guided modes and the external field, and the excitation of the GMR (see Figure S2a).[39] This GMR supports measurable resonances in the far field; i.e., it is a quasi-bound state. Importantly, excitation of GMRs only occurs for a small range of wavelengths, giving rise to strongly resonant fields and hence a high $Q$. For our first high-Q metalens design, we include periodic notches in the set of bars adjacent to the lens center (those with $w$ = 219 nm). For future experimental tractability, we consider notches that are 70 nm wide with a depth of $\delta$ = 50 nm and a period of 600 nm; such notches are well within reasonable fabrication parameters, as experimentally demonstrated by a recent high-Q, GMR beam steering platform,[40] while still giving large quality factors. This notch design gives rise to a GMR around a wavelength of 1500 nm.

We model the metalens using full field finite element simulations (COMSOL Multiphysics). We consider an incident $y$-polarized electric field with a Gaussian distribution incident from the $z$-direction. For an incident intensity of 0.1 mW/$\mu$m$^2$, the spectral response of the notched and unnotched metalenses is shown in Figure 1c. Note that the spectra are integrated over the area ($xy$-plane) at the designed focal length 4 $\mu$m from the metalens and are normalized to the mean of the unaltered Gaussian beam input. As seen, a high-Q resonance appears for the notched metasurface at a wavelength of $\lambda$ = 1499.4 nm, associated with a $Q$ factor of 3600. Near fields of the nanobars, shown in the insets of Figure 1c, show a maximum enhancement of the notched bar near a field intensity of 2.46 × 10$^4$ compared to the unnotched bars. Parts d and e of Figure 1 confirm the focusing abilities of the low-Q and high-Q metalenses for an incident wavelength of 1499.4 nm. For the low- and high-Q metasurfaces, the maximum focal intensity occurs at 4 and 3.9 $\mu$m, respectively, with full width at half-maxima (fwhm) of 1.22 $\mu$m (low $Q$) and 0.99 $\mu$m (high $Q$). Note that the higher focal intensity of the high-Q lens is not necessarily a product of the high-Q resonance. Nonetheless, our metasurface design simultaneously achieves strong focusing behavior as well as quality factors 2 orders of magnitude larger than those achieved by other diffractive metasurfaces; to our knowledge, this is the first high-Q metalens design.

As the incident power on the metalens increases, the nonlinear Kerr effect modifies the local permittivity according to $\varepsilon(r) = \varepsilon_0(\varepsilon_r + \chi^{(3)}|E(r)|^2)$; here, $E(r)$ is the local electric field strength, $\chi^{(3)}$ is the third-order nonlinear susceptibility, and $\varepsilon_r$ and $\varepsilon_0$ are the first-order permittivity of Si and vacuum, respectively. As the intensity increases from 0.1 to 1 mW/$\mu$m$^2$, we observe a redshift of the high-Q resonance from 1499.4 to 1499.9 nm, as shown in Figure 2a. This shift corresponds to a significant decrease in the far field enhancement of the focal


https://dx.doi.org/10.1021/acs.nanolett.0c01359
Nano Lett. 2020, 20, 5127−5132

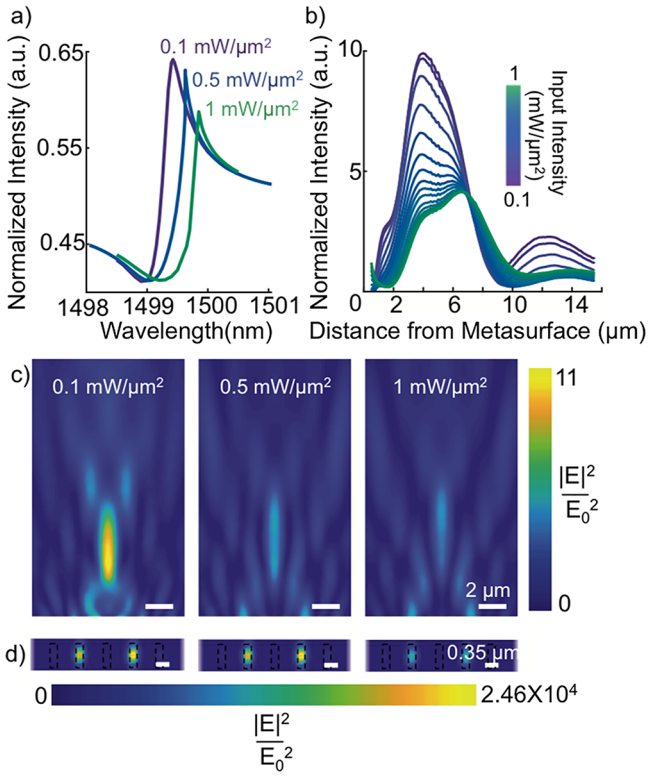


**Figure 2.** Nonlinear lens response. (a) Spectra calculated at the focal spot for input intensities of 0.1, 0.5, and 1 mW/$\mu$m$^2$. (b) Focal response in the propagation direction (along the $z$ axis above the high-Q metasurface) for various input intensities, revealing a shift of the focal length with increasing power. All plots are at a wavelength of 1499.4 nm. (c) $|E(r)|^2$ field plot for the nonlinear lens with input intensities of 0.1, 0.5, and 1 mW/$\mu$m$^2$. (d) Near field profiles within a section of the metasurface for the same powers and wavelengths shown in part c.

spot at $\lambda$ = 1499.4 nm, as the maximum of the low-power Fano resonance transitions to a minimum at high power. A resulting decrease of over 50% in the normalized focal intensity is observed with increasing input intensity, as shown in Figure S5a. A spatial change in the focal spot is also observed (Figure 2b). The focal intensity maximum shifts from 3.9 $\mu$m for an input intensity of 0.1 mW/$\mu$m$^2$ to 6.55 $\mu$m for an input intensity of 1 mW/$\mu$m$^2$; along with this shift in the maximum, the overall focal spot position (defined as the position where the focal spot is 0.2 times its maximum intensity—depicted in Figure S5c) shifts by ∼1.2 $\mu$m for the place the focal spot begins and ∼2.3 $\mu$m for the place the focal spot ends, with increasing input intensity.

The focusing power of the metalens at 1499.4 nm for low (0.1 mW/$\mu$m$^2$), mid (0.5 mW/$\mu$m$^2$), and high (1 mW/$\mu$m$^2$) input intensities is plotted in Figure 2c. These figures illustrate the power-limiting behavior for the nonlinear lens and the focal length shift. For both low-power and mid-power illumination, the near fields in the notched bars remain high, shown in Figure 2d; accordingly, the high-Q response in these cases is preserved. The high-Q response in the near field of the notched bars does begin to decrease by the highest intensity, as the resonance, the center of the high-Q response, has spectrally shifted; nonetheless, this decreased response still remains significant for the metalens overall. The Supporting Information includes further investigations of the nonlinear focusing at illumination intensities between 0.01 and 1 mW/$\mu$m$^2$. Based on the observed spectral resonance shifts and the onset of an appreciable power-limiting response, we estimate 0.1 mW/$\mu$m$^2$ as the nonlinear threshold, which saturates after approximately 1 mW/$\mu$m$^2$. As with similar high-Q resonant structures,[41,42] the efficiency of the nonlinear response is increased by at least 2 orders of magnitude, which reduces the necessary input powers to be experimentally reasonable.

Thus far, we have shown that only 2 nanobars out of 25 need to exhibit a GMR to induce an appreciable high-Q far-field response. Our high-Q scheme is extremely flexible: by changing either the nanobar or the perturbation geometry, we can tune the resonant wavelengths and high Q strength of our metasurface. We can further capitalize on this result via frequency-multiplexing, whereby multiple high-Q resonances can be simultaneously achieved by perturbing multiple pairs of nanobars. To demonstrate this possibility, we notch three bars on either side of the center of the lens simultaneously, all with a period of $p$ = 600 nm, as shown in Figure 3a. The notch period and geometry, in combination with the dispersion of the bars, will determine the resulting resonant wavelength.

For our high-Q multiplexed lens, we notch three sets of bars, with $w$ = 219, 205, and 158 nm, corresponding to the second, third, and fourth bars from the center of the lens (see Figure 3a). Though all nanobars are notched with a period of 600 nm, the resonances remain spectrally distinct, due to their differing guided mode wavevector (see Figure S2a). As before, the notches in the $w$ = 219 nm bars are 70 nm wide with a depth of $\delta_1$ = 50 nm; the notches in the $w$ = 205 nm bar have $\delta_2$ = 40 nm, while the notches in the $w$ = 158 nm bar have $\delta_3$ = 30 nm. Note that smaller perturbations generally correspond to higher Q factors for that resonance.[39]

Figure 3b shows the spectra of this multinotched metalens, depicting three distinct Fano resonant features. The resonance at $\lambda \sim$ 1500 nm exhibits a Q factor of approximately 3100 and enhancements in the $w$ = 219 nm notched bars of approximately 3.11 × 10$^4$, negligible in all other bars. The resonance at $\lambda \sim$ 1480 nm exhibits a Q factor of approximately 6700 and enhancements in the $w$ = 205 nm notched bars of approximately 3.05 × 10$^4$. Finally, the resonance at $\lambda \sim$ 1390 nm exhibits a Q factor of approximately 4700, with enhancements in the $w$ = 158 nm notched bars of approximately 3.57 × 10$^4$.

As with our singly resonant metalens, we explore the multinotched metasurface's nonlinear behavior. Redshifts in the high-Q resonances as the incident intensity is increased are seen in all cases, as reported in Figure S6. Accordingly, our high-Q metalens design supports frequency-multiplexed schemes. Figure 3 depicts field plots for the multinotched metalens for the low-power condition (left) and higher-power condition (right) for the lens operating at $\lambda_1$ = 1499.4 nm (d) and $\lambda_2$ = 1480.9 nm (e); the field profiles for $\lambda_3$ = 1388.45 nm are included as Figure S7a and b, as we note that the quality of the lensing decreases significantly due to chromatic aberrations at this wavelength so far from the optimal 1500 nm. For all wavelengths, power-limiting-like behavior is observed. More advanced metasurface designs, such as multilayered devices or dispersion engineering approaches,[43−45] could be readily employed to minimize these issues in the future. Importantly, such schemes would not negatively impact the high-Q nature of the metasurface, as the phase gradient characteristics of the metalens are designed separately, and thus largely decoupled, from the GMR design.


https://dx.doi.org/10.1021/acs.nanolett.0c01359
Nano Lett. 2020, 20, 5127−5132

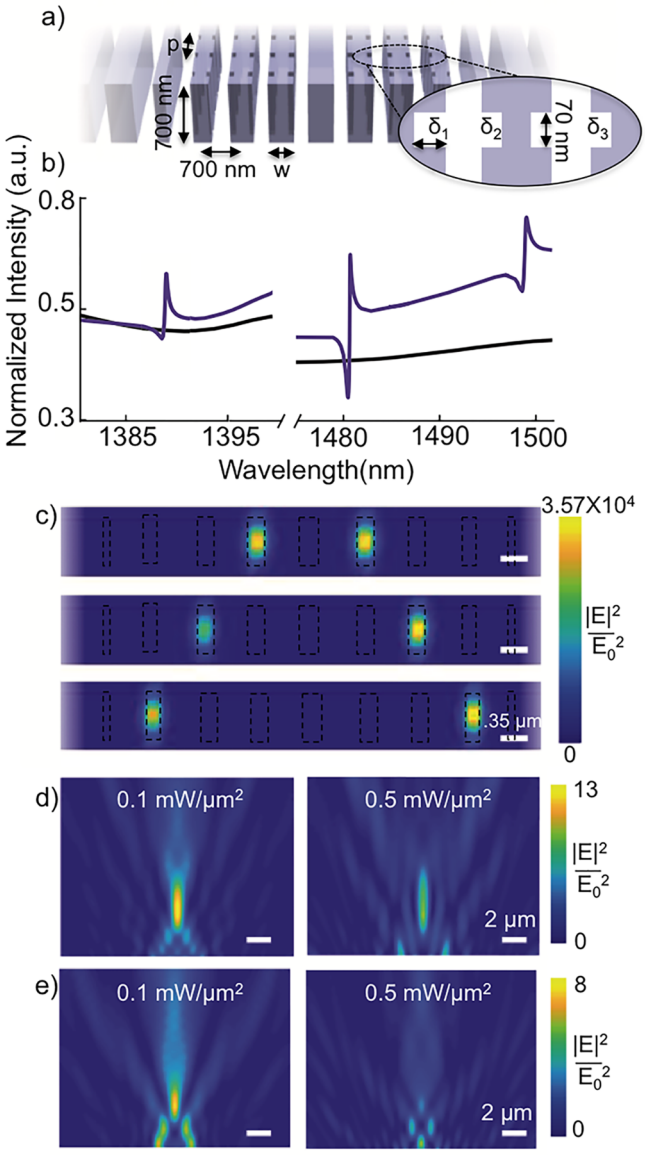


**Figure 3.** Multiplexed high-Q lenses. (a) Geometry of the multiwavelength resonant metalens; $p$ = 600 nm, $\delta_1$ = 50 nm, $\delta_2$ = 40 nm, $\delta_3$ = 30 nm, and $w$ varies for each bar according to Figure S1b. (b) Spectra of the unnotched (black) and notched (purple) lenses calculated at the focal spot, 4 $\mu$m from the metasurface, showing multiple resonant features. (c) Near-field profiles of the notched lens at wavelengths of 1499.4 nm (top), 1480.9 nm (middle), and 1399.45 (bottom). (d) $|E(r)|^2$ field plot for the nonlinear lens with an input intensity of 0.1 mW/$\mu$m$^2$ (left) and 0.5 mW/$\mu$m$^2$ (right), excited at $\lambda$ = 1499.4 nm. (e) $|E(r)|^2$ field plot for the nonlinear lens with an input intensity of 0.1 mW/$\mu$m$^2$ (left) and 0.5 mW/$\mu$m$^2$ (right), excited at $\lambda$ = 1480.9 nm.

In summary, we have designed the first high-Q metasurface lens that leverages its intrinsic nonlinear optical response for power-dependent modulation. Our design combines a diffractive metasurface with a high-Q guided mode resonance to enable efficient nonlinearities. With this metasurface, we show a near-infrared power-limiting-like response as well as changes in the focal spot of the lens. The design works at both single wavelengths and with multiple resonances at various wavelengths. Additionally, other functionalities,[46] such as aberration correction,[15−18] polarization detection,[47,48] or perturbation-based information storage and exchange,[49] could be implemented to augment the metalens function in future works. We note that centimeter-scale or longer focal lengths will require larger lenses. For these larger lenses, multiple pairs of bars could be notched to be resonant at the same wavelength (see Figure S2b), further increasing mode contrast and taking advantage of changes in the refractive index and phase response of multiple nanobars for the same operating wavelength. We anticipate that our high-Q metalenses will readily translate to a suite of dynamic imaging platforms, spanning LIFI, LIDAR, and wavefront sensing.

## ■ ASSOCIATED CONTENT

### Supporting Information

The Supporting Information is available free of charge at https://pubs.acs.org/doi/10.1021/acs.nanolett.0c01359.

Details of the lens design, guided mode dispersion, numerical simulations, nonlinear operation, and multi-notched/multiwavelength lensing response (PDF)

## ■ AUTHOR INFORMATION


### Corresponding Authors

**Elissa Klopfer** − *Department of Materials Science and Engineering, Stanford University, Stanford, California 94305, United States;* orcid.org/0000-0001-5153-1731; Email: eklopfer@stanford.edu

**Jennifer A. Dionne** − *Department of Materials Science and Engineering and Department of Radiology, Stanford University, Stanford, California 94305, United States;* orcid.org/0000-0001-5287-4357; Email: jdionne@stanford.edu

### Authors

**Mark Lawrence** − *Department of Materials Science and Engineering, Stanford University, Stanford, California 94305, United States;* orcid.org/0000-0002-0822-5453

**David R. Barton, III** − *Department of Materials Science and Engineering, Stanford University, Stanford, California 94305, United States*

**Jefferson Dixon** − *Department of Mechanical Engineering, Stanford University, Stanford, California 94305, United States;* orcid.org/0000-0003-4806-6984

Complete contact information is available at: https://pubs.acs.org/10.1021/acs.nanolett.0c01359


### Notes

The authors declare no competing financial interest.

## ■ ACKNOWLEDGMENTS

The authors would like to thank Jack Hu and Chris Siefe at Stanford as well as Zoran Jandric and Aditya Jain at Seagate Technology PLC for their useful feedback and advice on this manuscript. We acknowledge support from the Air Force Office of Scientific Research (Grant No. FA9550-15-1-0006, supporting M.L. and J.D.), the National Science Foundation (Grant No. DMR-1905209, supporting D.R.B. and J.D.). J.D. was supported by the Photonics at Thermodynamic Limits Energy Frontier Research Center funded by the U.S. Department of Energy, Office of Science, Office of Basic Energy Sciences, under Award No. DE-SC0019140. E.K. acknowledges support from a National Science Foundation Graduate Research Fellowship Program under Grant No. DGE-1656518.



https://dx.doi.org/10.1021/acs.nanolett.0c01359
Nano Lett. 2020, 20, 5127−5132

## REFERENCES


(1) Pfeiffer, C.; Grbic, A. Metamaterial Huygens' Surfaces: Tailoring Wave Fronts with Reflectionless Sheets. *Phys. Rev. Lett.* **2013**, *110*, 197401.

(2) Yu, N.; Capasso, F. Flat optics with designer metasurfaces. *Nat. Mater.* **2014**, *13*, 139−150.

(3) Mohammadi Estakhri, N.; Alu, A. Wave-front Transformation with Gradient Metasurfaces. *Phys. Rev. X* **2016**, *6*, 041008.

(4) Chen, X.; Huang, L.; Mühlenbernd, H.; Li, G.; Bai, B.; Tan, Q.; Jin, G.; Qui, C.-W.; Zhang, S.; Zentgraf, T. Dual-polarity plasmonic metalens for visible light. *Nat. Commun.* **2012**, *3*, 1198.

(5) Khorasaninejad, M.; Chen, W. T.; Devlin, R. C.; Oh, J.; Zhu, A. Y.; Capasso, F. Metalenses at visible wavelengths: Diffraction-limited focusing and subwavelength resolution imaging. *Science* **2016**, *352* (6290), 1190−1194.

(6) Li, B.; Piyawattanametha, W.; Qiu, Z. Metalens-Based Miniaturized Optical Systems. *Micromachines* **2019**, *10*, 310.

(7) She, A.; Zhang, S.; Shian, S.; Clarke, D. R.; Capasso, F. Large area metalenses: design, characterization, and mass manufacturing. *Opt. Express* **2018**, *26* (2), 1573−1585.

(8) Olson, J.; Manjavacas, A.; Basu, T.; Huang, D.; Schlather, A. E.; Zheng, B.; Halas, N. J.; Nordlander, P.; Link, Stephan *ACS Nano* **2016**, *10* (1), 1108−1117.

(9) Zhu, A. Y.; Chen, W. T.; Khorasaninejad, M.; Oh, J.; Zaidi, A.; Mishra, I.; Devlin, R. C.; Capasso, F. Ultra-compact visible chiral spectrometer with meta-lenses. *APL Photonics* **2017**, *2*, 036103.

(10) La Spada, L. Metasurfaces for Advanced Sensing and Diagnostics. *Sensors* **2019**, *19* (2), 355.

(11) Zhu, Y.; Li, Z.; Hao, Z.; DiMarco, C.; Maturavongsadit, P.; Hao, Y.; Lu, M.; Stein, A.; Wang, Q.; Hone, J.; Yu, N.; Lin, Q. Optical conductivity-based ultrasensitive mid-infrared biosensing on a hybrid metasurface. *Light: Sci. Appl.* **2018**, *7*, 67.

(12) Solomon, M. L.; Hu, J.; Lawrence, M.; Garcia-Etxarri, A.; Dionne, J. A. *ACS Photonics* **2019**, *6* (1), 43−49.

(13) Lee, G. Y.; Hong, J. Y.; Hwang, S. H.; Moon, S.; Kang, H.; Jeon, S.; Kim, H.; Jeong, J. H.; Lee, B. Metasurface eyepiece for augmented reality. *Nat. Commun.* **2018**, *9*, 4562.

(14) Li, Q.; van de Groep, J.; Wang, Y.; Kik, P. G.; Brongersma, M. L. Transparent multispectral photodetectors mimicking the human visual system. *Nat. Commun.* **2019**, *10*, 4982.

(15) Aieta, F.; Genevet, P.; Kats, M. A.; Yu, N.; Blanchard, R.; Gaburro, Z.; Capasso, F. Aberration-free ultrathin flat lenses and axicons at telecom wavelengths based on plasmonic metasurfaces. *Nano Lett.* **2012**, *12*, 4932−4936.

(16) Aieta, F.; Kats, M. A.; Genevet, P.; Capasso, F. Applied optics. Multiwavelength achromatic metasurfaces by dispersive phase compensation. *Science* **2015**, *347* (6228), 1342−1345.

(17) Wang, S.; Wu, P. C.; Su, V.-C.; Lai, Y.-C.; Chen, M.-K.; Kuo, H. Y.; Chen, B. H.; Chen, Y. H.; Huang, T.-T.; Wang, J.-H.; Lin, R.-M.; Kuan, C.-H.; Li, T.; Wang, Z.; Zhu, S.; Tsai, D. P. A broadband achromatic metalens in the visible. *Nat. Nanotechnol.* **2018**, *13*, 227−232.

(18) Chen, W. T.; Zhu, A. Y.; Sanjeev, V.; Khorasaninejad, M.; Shi, Z.; Lee, E.; Capasso, F. A broadband achromatic metalens for focusing and imaging in the visible. *Nat. Nanotechnol.* **2018**, *13*, 220−226.

(19) Chen, W. T.; Zhu, A. Y.; Sisler, J.; Bharwani, Z.; Capasso, F. A broadband achromatic polarization-insensitive metalens consisting of anisotropic nanostructures. *Nat. Commun.* **2019**, *10*, 355.

(20) Wang, Q.; Rogers, E. T. F.; Gholipour, B.; Wang, C.-M.; Wang, G.; Teng, J.; Zheludev, N. I. Optically reconfigurable metasurfaces and photonic devices based on phase change materials. *Nat. Photonics* **2016**, *10*, 60−65.

(21) Yin, X.; Steinle, T.; Huang, L.; Taubner, T.; Wuttig, M.; Zentgraf, T.; Giessen, H. Beam switching and bifocal zoom lensing using active plasmonic metasurfaces. *Light: Sci. Appl.* **2017**, *6*, No. e17016.

(22) Kim, Y.; Wu, P. C.; Sokhoyan, R.; Mauser, K.; Glaudell, R.; Shirmanesh, G. K.; Atwater, H. A. Phase modulation with electrically tunable vanadium dioxide phase-change metasurfaces. *Nano Lett.* **2019**, *19*, 3961−3968.

(23) Yao, Y.; Shankar, R.; Kats, M. A.; Song, Y.; Kong, J.; Loncar, M.; Capasso, F. Electrically tunable metasurface perfect absorbers for ultrathin mid-infrared optical modulators. *Nano Lett.* **2014**, *14* (11), 6526−32.

(24) Kafaie Shirmanesh, G.; Sokhoyan, R.; Pala, R. A.; Atwater, H. A. Dual-gated active metasurface at 1550 nm with wide (>300°) phase tunability. *Nano Lett.* **2018**, *18*, 2957−2963.

(25) Wu, P.; Pala, R. A.; Kafaie Shirmanesh, G.; Cheng, W. H.; Sokhoyan, R.; Grajower, M.; Alam, M. Z.; Lee, D.; Atwater, H. A. Dynamic beam steering with all-dielectric electro- optic III-V multiple-quantum-well metasurfaces. *Nat. Commun.* **2019**, *10*, 3654.

(26) Sherrott, M. C.; Hon, P. W.C.; Fountaine, K. T.; Garcias, J. C.; Pontis, S. M.; Brar, V. W.; Sweatlock, L. A.; Atwater, H. A. *Nano Lett.* **2017**, *17* (5), 3027−3034.

(27) Brouillet, J.; Papadakis, G. T.; Atwater, H. A. Experimental demonstration of tunable graphene-polaritonic hyperbolic metamaterial. *Opt. Express* **2019**, *27*, 30225−30232.

(28) Kowerdziej, R.; Olifierczuk, M.; Parka, J.; Wrobel, J. Terahertz characterization of tunable metamaterial based on electrically controlled nematic liquid crystal. *Appl. Phys. Lett.* **2014**, *105*, 022908.

(29) Zhong, J.; An, J.; Yi, N.; Zhu, N.; Song, M.; Xiao, Q. S. Broadband and Tunable-Focus Flat Lens with Dielectric Metasurface. *Plasmonics* **2016**, *11*, 537.

(30) Komar, A.; Paniagua-Dominguez, R.; Miroshnichenko, A.; Yu, Y. F.; Kivshar, Y. S.; Kuznetsov, A. I.; Neshe, D. Dynamic beam switching by liquid crystal tunable dielectric metasurfaces. *ACS Photonics* **2018**, *5*, 1742−1748.

(31) Li, S.-Q.; Xu, X.; Veetil, R. M.; Valuckas, V.; Paniagua-Dominguez, R.; Kuznetsov, A. I. Phase-only transmissive spatial light modulator based on tunable dielectric metasurface. *Science* **2019**, *364* (6445), 1087−1090.

(32) Ou, J.-Y.; Plum, E.; Zhang, J.; Zheludev, N. I. An electromechanically reconfigurable plasmonic metamaterial operating in the near-infrared. *Nat. Nanotechnol.* **2013**, *8*, 252−255.

(33) Ee, H. S.; Agarwal, R. Tunable Metasurface and Flat Optical Zoom Lens on a Stretchable Substrate. *Nano Lett.* **2016**, *16* (4), 2818−2823.

(34) She, A.; Zhang, S.; Shian, S.; Clarke, D. R.; Capasso, F. Adaptive metalenses with simultaneous electrical control of focal length, astigmatism, and shift. *Sci. Adv.* **2018**, *4*, No. eaap9957.

(35) Arbabi, E.; Arbabi, A.; Kamali, S. M.; Horie, Y.; Faraji-Dana, M.; Faraon, A. MEMS-tunable dielectric metasurface lens. *Nat. Commun.* **2018**, *9*, 812.

(36) Holsteen, A. L.; Cihan, A. F.; Brongersma, M. L. Temporal color mixing and dynamic beam shaping with silicon metasurfaces. *Science* **2019**, *365*, 257−260.

(37) Leuthold, J.; Koos, C.; Freude, W. Nonlinear silicon photonics. *Nat. Photonics* **2010**, *4* (8), 535−544.

(38) Yang, Y.; Wang, W.; Boulesbaa, A.; Kravchenko, I. I.; Briggs, D. P.; Puretzky, A.; Geohegan, D.; Valentine, J. Nonlinear Fano-Resonant Dielectric Metasurfaces. *Nano Lett.* **2015**, *15*, 7388.

(39) Lawrence, M.; Barton, D. R.; Dionne, J. Nonreciprocal flat optics with silicon metasurfaces. *Nano Lett.* **2018**, *18*, 1104−1109.

(40) Lawrence, M., Barton, D. R., Dixon, J., Song, J., van de Groep, J., Brongersma, M., Dionne, J. High Quality Factor Phase Gradient Metasurfaces. *Nat. Nanotechnol.*, in press.

(41) Koshelev, K.; Bogdanov, A.; Kivshar, Y. Boosting Second-Harmonic Generation in Nonlinear Metasurfaces with Bound States in the Continuum. *Conference on Lasers and Electro-Optics* 2019, OSA Technical Digest.

(42) Xiao, Y.-F.; Ozdemir, S. K.; Gaddam, V.; Dong, C.-H.; Imoto, N.; Yang, L. Quantum nondemolition measurement of photon number via optical Kerr effect in an ultra-high-Q microtoroid cavity. *Opt. Express* **2008**, *16*, 21462−21475.

(43) Zhu, A. Y.; Chen, W. T.; Sisler, J.; Yousef, K. M. A.; Lee, E.; Huang, Y.-W.; Qiu, C.-W.; Capasso, F. Compact Aberration-




https://dx.doi.org/10.1021/acs.nanolett.0c01359
*Nano Lett.* 2020, 20, 5127−5132

Corrected Spectrometers in the Visible Using Dispersion-Tailored Metasurfaces. *Adv. Opt. Mater.* **2019**, *7*, 1801144.
(44) Zhou, Y.; Kravchenko, I. I.; Wang, H.; Zheng, H.; Gu, G.; Valentine, J. Multifunctional metaoptics based on bilayer metasurfaces. *Light: Sci. Appl.* **2019**, *8*, 80.
(45) Zhou, Y.; Kravchenko, I. I.; Wang Hao Nolen, J. R.; Gu, G.; Valentine, J. Multilayer Noninteracting Dielectric Metasurfaces for Multiwavelength Metaoptics. *Nano Lett.* **2018**, *18* (12), 7529−7537.
(46) Kamali, S. M.; Arbabi, E.; Arbabi, A.; Horie, Y.; Faraji-Dana, M.; Faraon, A. Angle-multiplexed metasurfaces: encoding independent wavefronts in a single metasurface under different illumination angles. *Phys. Rev. X* **2017**, *7*, 041056.
(47) Khorasaninejad, M.; Chen, W. T.; Zhu, A. Y.; Oh, J.; Devlin, R. C.; Rousso, D.; Capasso, F. Multispectral Chiral Imaging with a Metalens. *Nano Lett.* **2016**, *16* (7), 4595−4600.
(48) Rubin, N. A.; D'Aversa, G.; Chevalier, P.; Shi, Z.; Chen, W. T.; Capasso, F. Matrix Fourier optics enables a compact full-Stokes polarization camera. *Science* **2019**, *365*, eaax1839.
(49) Xue, J.; Zhou, Z.; Lin, L.; Guo, C.; Sun, S.; Lei, D.; Qui, C.; Wang, X. Perturbative countersurveillance metaoptics with compound nanosieves. *Light: Sci. Appl.* **2019**, *8*, 101.



https://dx.doi.org/10.1021/acs.nanolett.0c01359
*Nano Lett.* 2020, 20, 5127−5132